第 32 卷第 7 期
2016 年 7 月

无 机 化 学 学 报
CHINESE JOURNAL OF INORGANIC CHEMISTRY

Vol.32 No.7
1246-1254

单分散 g-C_3N_4 量子点修饰一维棒状 $BiPO_4$ 微晶的合成及其对光催化活性增强机理

王丹军*,[1] 申会东[1] 郭 莉[1,2] 岳林林[1] 付 峰*,[1]

([1]延安大学化学与化工学院,陕西省化学反应工程重点实验室,延安 716000)

([2]陕西师范大学材料科学与工程技术学院,西安 716000)

摘要:利用水热法合成了一维棒状 $BiPO_4$ 微晶,在此基础上采用浸渍–焙烧法进行 g-C_3N_4 量子点表面修饰获得新颖的 g-C_3N_4/$BiPO_4$ 异质结。借助 X 射线衍射(XRD)、场发射扫描电镜(FE-SEM)、透射电镜(HRTEM)、能谱(EDS)、紫外–可见漫反射(UV-Vis-DRS)等测试手段对所得样品的相组成、形貌和谱学特征进行了表征。选择罗丹明 B(RhB)和苯酚作为模型污染物研究了所得在可见光下的催化活性。结果表明,样品 16%(*w*/*w*) g-C_3N_4/$BiPO_4$ 对 RhB 降解的速率常数分别是纯 g-C_3N_4 和 $BiPO_4$ 的 4.6 倍和 15 倍。g-C_3N_4 量子点与 $BiPO_4$ 之间形成异质结,抑制了光生电子–空穴对的复合,从而提高了催化剂的活性。自由基捕获实验进一步表明,超氧负离子自由基($\cdot O_2^-$)是催化降解 RhB 和苯酚的主要活性物种。

关键词:一维棒状 $BiPO_4$ 微晶;g-C_3N_4 量子点;表面修饰;活性增强机理

中图分类号:O647.32 **文献标识码**:A **文章编号**:1001-4861(2016)07-1246-09

DOI:10.11862/CJIC.2016.170

Synthesis of Monodispersed g-C_3N_4 Quantum Dots (QDs) Decorated on the Surface of 1D Rod-like $BiPO_4$ with Enhanced Photocatalytic Activities

WANG Dan-Jun*,[1] SHEN Hui-Dong[1] GUO Li[1,2] YUE Lin-Lin[1] FU Feng*,[1]

([1]*College of Chemistry &Chemical Engineering, Yan'an University, Shaanxi Key Laboratory of Chemical Reaction Engineering, Yan'an, Shaanxi* 716000, *China*)

([2]*School of Materials Science and Engineering, Shaanxi Normal University, Xi'an* 710119, *China*)

Abstract: 1D rod-like $BiPO_4$ have been successfully synthesized via a hydrothermal process, and g-C_3N_4 quantum dots (QDs) was decorated on the surface of $BiPO_4$ to form a novel g-C_3N_4/$BiPO_4$ heterojunction via a followed impregnation-calcinations method. XRD, FE-SEM, HR-TEM, EDS and UV-Vis-DRS techniques were employed to characterize the phase composition, morphology and spectrum properties of as-synthesized samples. The photocatalytic activities of samples were evaluated by degradation of RhB and phenol under visible light irradiation. The results also shows that 16%(*w*/*w*) g-C_3N_4/$BiPO_4$ photocatalysts possesses the maximal k value of 0.348 min^{-1}, which is 15 and 4.6 times higher than that of pure $BiPO_4$ and g-C_3N_4, respectively. The catalytic efficiency enhancement of g-C_3N_4/$BiPO_4$ heterojunctions relative to pure-$BiPO_4$ can be attributed to the formation of heterojunctions between g-C_3N_4 QDs and $BiPO_4$, which suppresses the recombination of photogenerated electron-holes. The radical scavengers test further confirmed that $\cdot O_2^-$ was the main reactive species during the

收稿日期:2016-01-02。收修改稿日期:2016-05-23。

国家自然科学基金(No.21373159)、陕西省科技项目(No.2013K11-08,2013SZS20-P01,2015YG174)、陕西省教育厅科研基金项目(No.15JS119)、延安大学基金(No.2013YDZ-07,YDBK2013-11)和延安大学研究生科研创新项目(No.YCX201602)资助项目。

*通信联系人。E-mail:wangdj761118@163.com,FengFu@126.com

photocatalytic process. Therefore, this work provides a facile process for the design of novel and efficient $BiPO_4$-based photocatalyst with multi-components.

Keywords: rod-like $BiPO_4$ microcrystal; g-C_3N_4 quantum dots (QDs); decoration; photocatlaytic activity enhancement mechanism

0 Introduction

During the past few decades, semiconductor-based photocatalysis has been widely investigated for its potential application in environmental remediation and solar energy transformation. Up to date, the most strategy to construct efficient visible-responsive photocatalyst is to extend the light absorption range, and prolong the life of photogenerated charge carriers by element doping and surface modification[1-3]. Unfortunately, element doping is difficult to be controlled, and low thermal stability, which limits its application[4-5]. Therefore, the surface modification has become an important strategy is to develop more efficient photocatalyst with visible light responsiveness and low recombination rate of photogenerated electron and holes[6-8].

As one of an important Bi-based photocatalyst materials, $BiPO_4$ has received much attention owing to it potential applications as a oxy-acid salt photocatalyst with wide band-gap and high separation efficiency of e^-/h^+ pairs[9]. Moreover, PO_4^{3-} helps the e^-/h^+ separation, which plays an important role in its excellent photocatlaytic activity. However, the potential application of $BiPO_4$ is limited by inherent constraints such as inefficient use of the visible portion and low lifetime of photogenerated carriers. So, the photocatalytic efficiency of $BiPO_4$ needs further enhancement prior to practical applications[10-13]. Graphitic carbon nitride (g-C_3N_4) is a novel metal free organic photocatalyst with a narrow band gap of 2.7 eV[14], which make it can utilize visible light directly. In addition, g-C_3N_4 is extremely stable owing to its tristriazine-ring structure and high degree of condensation[15]. So, it has been widely used as a narrow band gap semiconductor to construct hetero-photocatalyst by coupling over wider band gap semiconductor photocatalyst. Recently, Zhu′s groups have prepared the core/hell structured g-C_3N_4/$BiPO_4$ photocatalyst via ultrasonic dispersion method [16]. Although core/hell structured g-C_3N_4/$BiPO_4$ exhibits high photocatalytic activities, the preparation process is high energy consumption. So, it′s vital to explore the facile and practicable method for fabrication g-C_3N_4/$BiPO_4$ photocatalyst. Very recently, Li et al. reported a spherical g-C_3N_4/$BiPO_4$ composite via a associated sonochemical and heat-treating process and the experimental results revealed that g-C_3N_4/$BiPO_4$ exhibited high photocatalytic activity for methyl orange[17]. The above work inspired us to construct g-C_3N_4/$BiPO_4$ composite photocatalyst and investigate it activity enhancement mechanism.

Very recently, we have successfully fabricated AgBr/$BiPO_4$ heterojunction by loading AgBr QDs on the surface of $BiPO_4$ microcrystals[18]. In this work, one-dimensional (1D) rod-like $BiPO_4$ was designed and fabricated by the hydrothermal method according to our previous report[18-19]. Then, g-C_3N_4 QDs was decorated on the surface of rod-like $BiPO_4$ to construct the novel heterojunctions via the followed impregnation-calcinations process. Furthermore, the mechanism of enhanced catalytic activity for g-C_3N_4/$BiPO_4$ heterojunctions was also discussed.

1 Experimental section

1.1 Sample preparation

All reagents were analytical purity and received without further purification. Rod-like $BiPO_4$ microcrystal was prepared according to our previous report[18-19]. In a typical process, 5 mmol $Bi(NO_3)_3 \cdot 5H_2O$ was dissolved in 5 mL HNO_3 (4.0 mol·L^{-1}), then $NH_4H_2PO_4$ solution were slowly added to above $Bi(NO_3)_3$ solution drop-wise under vigorously stirring. Afterward, the suspension was transported into 50 mL Teflon-lined autoclave and heated at 190 ℃ for 24 h. After hydrothermal reaction, the autoclave was naturally cooled to room temperature. Then, the resulted

precipitates were collected, washed with deionized water and absolute ethanol for several times, and dried in a vacuum oven at 80 ℃ for 4 h.

The g-C_3N_4/$BiPO_4$ were obtained by a simple impregnation-calcinations process method. In a typical procedure, a certain amount of melamine was dissolved in methanol. Then, 1.0 g as-prepared $BiPO_4$ was dispersed in the above solution and vigorously stirred for 60 min to obtain a uniform suspension and then dried to get dry powder. Finally, the powder was heated to 550 ℃ with speed of 2 ℃·min^{-1} in muffle furnace, then kept for 4 h, and the resulted powders were ground for further use. According to above method, the contents of g-C_3N_4 in g-C_3N_4/$BiPO_4$ heterojunction range from 2.0% to 20.0% (*w*/*w*, the same below) were prepared.

1.2 Characterizations

X-ray diffraction (XRD) patterns were measured with a Shimadzu XRD-7000 X-ray diffractometer using Cu *Kα* radiation. Scanning electron microscopy (SEM) images and energy dispersive X-ray spectroscopy (EDS) maps were obtained with a Hitachi a JEOL JSM-6610LV field emission scanning electron microscope. Transmission electron microscopy (TEM) observations were performed on a JEOL JEM-2100 electron microscope with an accelerating voltage of 200 kV. Diffuse reflectance spectra (UV-Vis-DRS) of the samples were recorded on a Shimadzu UV-2550 UV-Visible spectrometer using $BaSO_4$ as the reference.

1.3 Photocatalytic activity test

The photocatalytic activities of samples were evaluated by degradation rhodamine B (RhB) and phenol under visible light irradiation of a 400 W metal halide lamp with a cutoff filter to cut off the light below 420 nm. The experiment detail was similar to our previous report[18]. Chemical oxygen demand (COD) was determined at a COD rapid monitor (5B-3B, LanHua Co., LTD, China). To investigate the active species generated in the photocatalytic system, different scavengers, including tertiary butanol (TBA, 10 mmol·L^{-1}), benzoquinone (BQ), ethylenediamine tetraacetic acid disodium salt (EDTA-2Na, 10 mmol·L^{-1})[20-22], were introduced into the photocatalysis solution to examine ·OH, O_2^{-}· and h^+, respectively. The experimental procedures were conducted as follows: 200 mg of photocatalyst and 200 mL fresh aqueous solution of RhB was continuously magnetically stirred in dark for 1.0 h to establish an adsorption/desorption equilibrium of solution. Then, scavenger was added into the solution to obtained a concentration of 10 mmol·L^{-1}. At given irradiation time intervals, then, 5 mL of the suspension were sampled, centrifuged to remove the catalyst particles, and measured the concentration of RhB.

2 Result and discussion

2.1 XRD, SEM and EDS of g-C_3N_4/$BiPO_4$

Fig.1 exhibited the XRD patterns of as-prepared samples. It is clearly seen that the diffraction peaks of samples could be assigned to orthorhombic g-C_3N_4 (JCPDS No.08-0209) and monoclinic $BiPO_4$ (JCPDS No.89-0287)[13,16]. Because some characteristic perks of g-C_3N_4 were near those of $BiPO_4$, the intensity changes in the $BiPO_4$ peaks were not obvious. In comparison, the intensities of the peaks at 29.08 was clearly raised in the g-C_3N_4/$BiPO_4$ composites with an increasing amount of g-C_3N_4. Meanwhile, no impurities were detected, indicating the high purity of the obtained samples.

The morphology of the as-synthesized pure-$BiPO_4$, g-C_3N_4, and g-C_3N_4/$BiPO_4$ composites were observed by SEM. As shown in Fig.2a ~b, $BiPO_4$

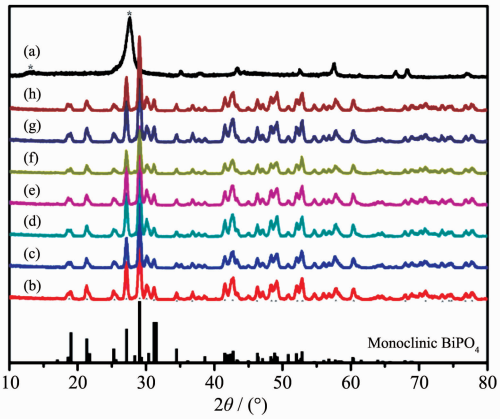

(a) g-C_3N_4; (b) $BiPO_4$; (c) 2.0% g-C_3N_4/$BiPO_4$; (d) 4.0% g-C_3N_4/$BiPO_4$; (e) 8.0% g-C_3N_4/$BiPO_4$; (f) 10.0% g-C_3N_4/$BiPO_4$; (g) 16.0% g-C_3N_4/$BiPO_4$; (h) 20.0% g-C_3N_4/$BiPO_4$

Fig.1 XRD patterns of g-C_3N_4/$BiPO_4$ samples

exhibited an 1D rod-like shape with smooth surface. In order to form g-C_3N_4/$BiPO_4$ heterojunctions, g-C_3N_4 QDs were loaded onto the surface of the rod-like $BiPO_4$ microcrystals (Fig.2b). The morphology of g-C_3N_4/$BiPO_4$ was not changed obviously because the g-C_3N_4 content was very low, but g-C_3N_4/$BiPO_4$ microrod become wider than pure $BiPO_4$. Further information g-C_3N_4/$BiPO_4$ heterojunctions was obtained for TEM images (Fig.2c~d). The locations of g-C_3N_4 nanoparticles on the surface of rod-like $BiPO_4$ are indicated by

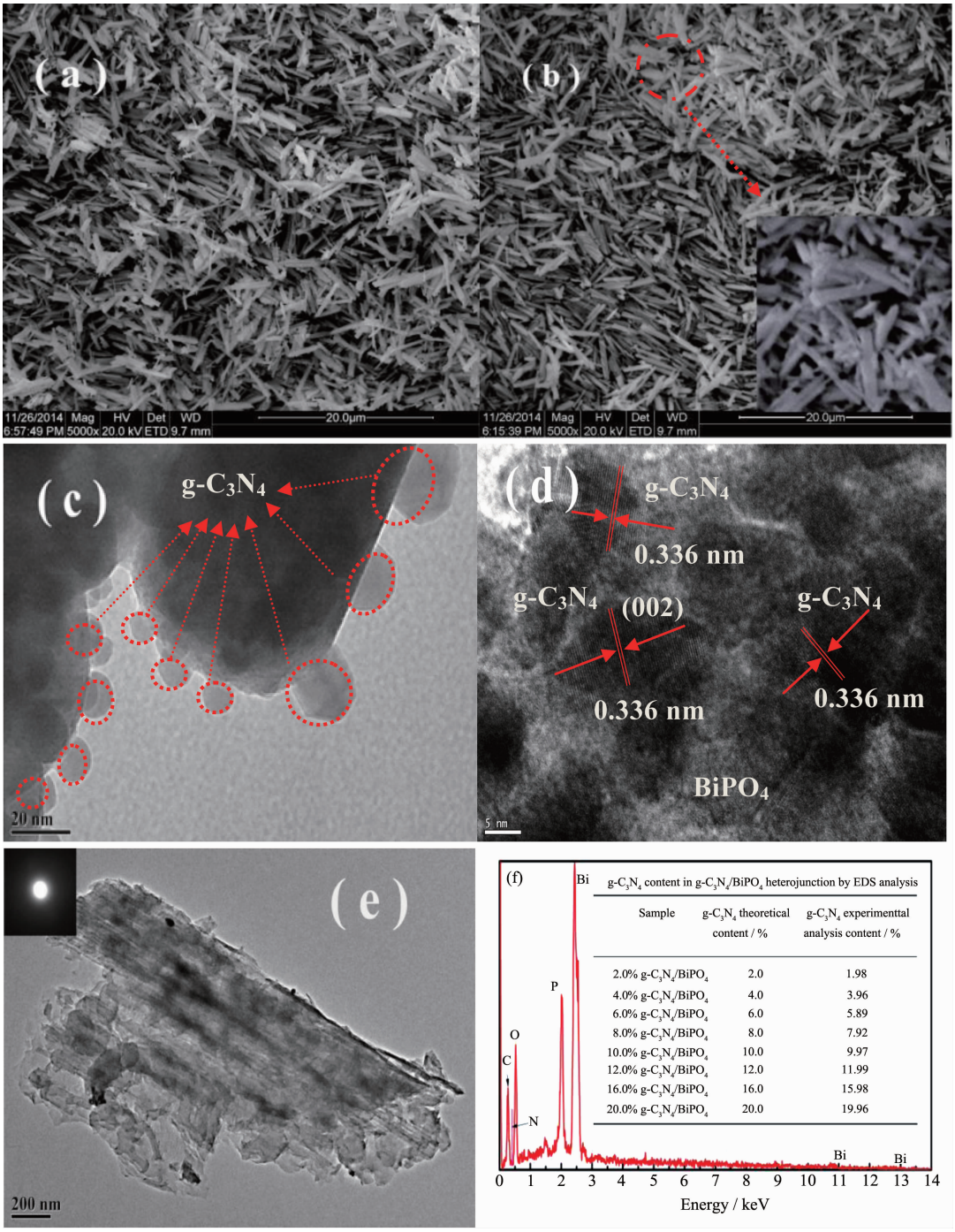

g-C_3N_4 content in g-C_3N_4/$BiPO_4$ heterojunction by EDS analysis

Sample	g-C_3N_4 theoretical content / %	g-C_3N_4 experimenttal analysis content / %
2.0% g-C_3N_4/$BiPO_4$	2.0	1.98
4.0% g-C_3N_4/$BiPO_4$	4.0	3.96
6.0% g-C_3N_4/$BiPO_4$	6.0	5.89
8.0% g-C_3N_4/$BiPO_4$	8.0	7.92
10.0% g-C_3N_4/$BiPO_4$	10.0	9.97
12.0% g-C_3N_4/$BiPO_4$	12.0	11.99
16.0% g-C_3N_4/$BiPO_4$	16.0	15.98
20.0% g-C_3N_4/$BiPO_4$	20.0	19.96

(a) SEM images pure-$BiPO_4$ and (b) 16.0%g-C_3N_4/$BiPO_4$ heterojunction(the inset picture in right corner is the enlarge image of circle); (c) TEM image of 16%g-C_3N_4/$BiPO_4$; (d) HRTEM of g-C_3N_4/$BiPO_4$ heterojunctions; (e) TEM image of g-C_3N_4; (f) EDS spectrum of 16.0%g-C_3N_4/$BiPO_4$ heterojunction (inset table shows the g-C_3N_4 content)

Fig.2　SEM and TEM images of samples

arrows in the TEM images (Fig.2c). It reveals that high dispersed spherical heteroparticles with size of about 20 nm loaded the surface of rod-like $BiPO_4$. Fig.2d show the lattice fringe of 0.336 nm, corresponding to the (002) plane of g-C_3N_4, is clearly observed in the g-C_3N_4/$BiPO_4$ composite and that the interfaces between g-C_3N_4 and $BiPO_4$ are smooth, which further verifies the formation of a g-C_3N_4/$BiPO_4$ heterojunction. In addition, it is observation from Fig.2e that pure g-C_3N_4 displays plate-like shape morphology. SEM and TEM information clearly exhibited that g-C_3N_4 QDs were highly dispersed on the surface of $BiPO_4$ and form the novel heterojunction structure. Fig.2f indicated that the content of g-C_3N_4 in g-C_3N_4/$BiPO_4$ in the samples were also close to the theoretical calculated value of g-C_3N_4/$BiPO_4$ (inset picture in Fig. 2f).

2.2 UV-Vis-DRS analysis

UV-Vis DRS spectra of the as-obtained samples are shown in Fig.3. According to Fig.3a, the absorption edge of pure-$BiPO_4$ and g-C_3N_4 are occurred at about 320 nm and 465 nm, respectively. Moreover, the g-C_3N_4/$BiPO_4$ composites presented similar absorption characteristics to pure $BiPO_4$ due to the low content g-C_3N_4 of in g-C_3N_4/$BiPO_4$ heterojunction. The efficient visible light absorption abilities ensured that g-C_3N_4/$BiPO_4$ generated sufficient electron-hole pairs under visible light irradiation. In addition, the band gap energies (E_g) of g-C_3N_4 and $BiPO_4$ were calculated according to the formula: $(\alpha h\gamma)^2=A\ (h\nu-E_g)$, where α, h, ν, A and E_g stand for the absorption coefficient, Planck′s constant, the light frequency, a constant and band gap energy, respectively[17,19]. Therefore, the corresponding E_g values of g-C_3N_4, $BiPO_4$ and 16.0% g-C_3N_4/$BiPO_4$ were determined from a plot of $(\alpha h\nu)^2$ versus energy ($h\nu$) (Fig.3b) and estimated to be 2.6, 3.85 and 3.82 eV, respectively.

2.3 Photocatalytic activity

The photocatalytic activities of the samples were evaluated by the degradation of RhB and phenol under visible light irradiation. The photocatalytic reactions follow pseudo-first-order kinetics law according to the Langmuir-Hinshelwood model for low concentration pollutant. The kinetics equation can be expressed as follows[23]: $\ln(C_0/C_t)=kt+\ln(C_0/C_1)$, where k is the pseudo-first-order rate constant, C_0 is the original concentration of RhB or phenol (10 mg·L^{-1}), C_1 is the concentration after adsorption, and C_t represents the concentration at reaction time t. It can be seen from Fig.4a that the photocatalytic activity is enhanced gradually with the content of g-C_3N_4 increasing from 4% to 16%. However, further increasing the content of g-C_3N_4 in the heterojunctions leads to a decrease in the degradation rate. This result may be attributed to the agglomera-tion of g-C_3N_4 QDs in the surface of $BiPO_4$, which can weaken the heterojunction structure and decrease the catalytic activity [24-25]. Therefore, a suitable ratio and well dispersion of g-C_3N_4 QDs in the composites are necessary. From Fig.4a, it also can be seen that pure-$BiPO_4$ can decompose 12.5% of RhB

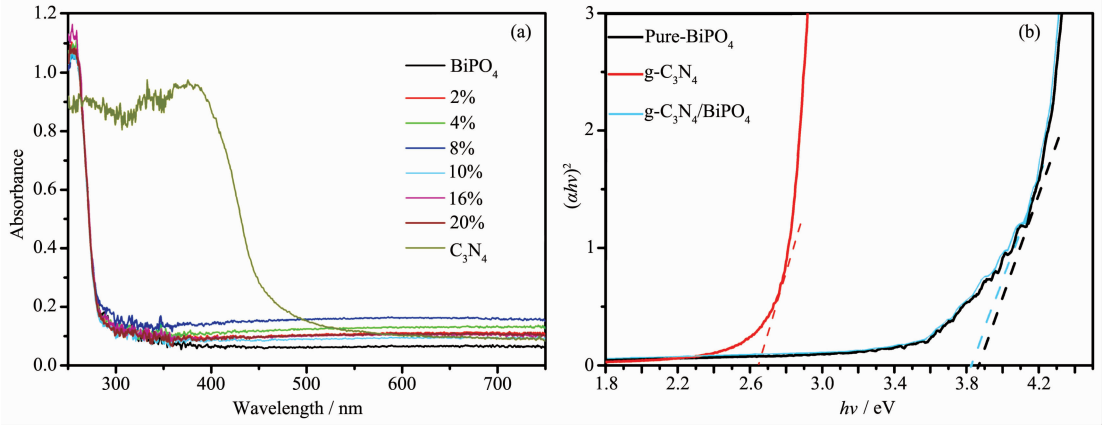

Fig.3 UV-Vis-DRS spectra of the as-obtained samples(a) and the band gap energies (E_g) of $BiPO_4$, g-C_3N_4 and 16.0% g-C_3N_4/$BiPO_4$ heterojunction (b)

after 10 min illumination. Significantly, g-C_3N_4/$BiPO_4$ composites exhibited improved photocatalytic activities compared to pure $BiPO_4$ and pure g-C_3N_4. In particular, 16.0% g-C_3N_4/$BiPO_4$ showed the best photocatalytic activity than those of the others, corresponding to 97.85% of RhB with 10 min illumination. Fig.4b show the k value obtained from the fitted straight-line plots of $\ln(C_t/C_0)$ versus time(t), which follow the order: pure-$BiPO_4$<4.0% g-C_3N_4/$BiPO_4$<8.0% g-C_3N_4/$BiPO_4$<10.0% g-C_3N_4 /$BiPO_4$<20.0% g-C_3N_4/$BiPO_4$<16.0% g-C_3N_4/$BiPO_4$. The results shows that 16% g-C_3N_4/$BiPO_4$ photocatalysts possesses the maximal k value of 0.348 min^{-1}, which is 15 and 4.6 times higher than that of pure $BiPO_4$ and g-C_3N_4, respectively. Moreover, phenol was chosen as another model environmental organic pollutant to further evaluate photocatalytic activity of g-C_3N_4 QDs decorated rod-like $BiPO_4$ also investigated (Fig.5a~b). Similar to the RhB results, the g-C_3N_4 QDs decoration on the surface results in an increase of phenol degradation. 16% g-C_3N_4/$BiPO_4$ heterostructure also shows the best activity, with constants k=0.178 min^{-1}. Fig.6 shows that the COD removal ratio of 16% g-C_3N_4/$BiPO_4$ reaches a value of 87.8% after 60 min of irradiation, while that of pure-$BiPO_4$ and g -C_3N_4 is 37.9% and 45.5%, respectively. The COD value reduction of 16% g-C_3N_4/$BiPO_4$ is slower than that of degradation of phenol. It is well-known that mineralization of organic compounds through two steps: ring cleavage and subsequently the oxidation of fragments. In our experiment, the COD removal rate of 16.0% g-C_3N_4/$BiPO_4$ exhibits different behavior before and after 20 min of irradiation. These results confirm that phenol is first ring cleaved and then converted to CO_2 and H_2O. The loss of COD via mineralization can be lowered more than the removed amount of organic pollutants because these parent molecules are decomposed to smaller organic intermediates, and further degradation of these intermediates to CO_2 and

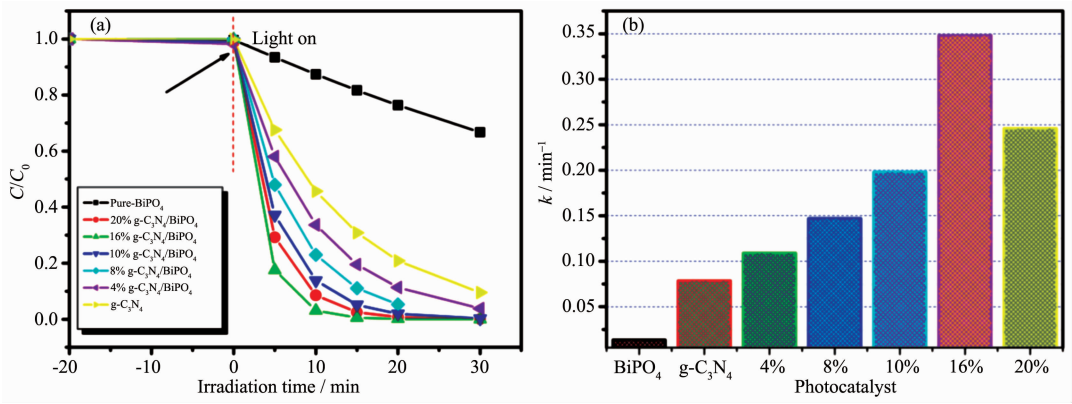

Fig.4　Photocatalytic activities of the prepared g-C_3N_4/$BiPO_4$ heterostructure for the RhB (a) and Corresponding k values of the different photocatalysts (b) under visible-light irradiation

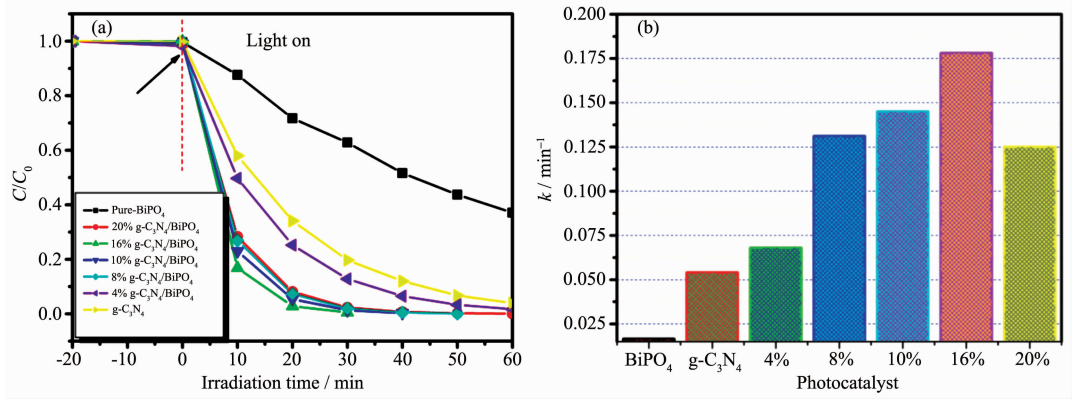

Fig.5　Photocatalytic activities of the g-C_3N_4/$BiPO_4$ composite photocatalysts for the phenol (a) and the corresponding k values of the different photocatalysts (b) under visible-light irradiation

Table 1 S_{BET} value and photocatalytic activities of g-C_3N_4/$BiPO_4$ heterojunctions

Sample	S_{BET} / ($m^2 \cdot g^{-1}$)	Rate constant k for RhB / min^{-1}	$\ln(C_0/C_1)$	COD removal at 60 min for RhB / %	$\ln(C_0/C_1)$	Rate constant k for phenol / min^{-1}	COD removal at 60 min for phenol / %
pure-$BiPO_4$	4	0.0135	0.010	29.8	0.011	0.0065	37.9
g-C_3N_4	19	0.0465	0.020	40.2	0.012	0.054	45.5
4.0% g-C_3N_4/$BiPO_4$	4	0.0784	0.021	56.2	0.011	0.067	56.6
8.0% g-C_3N_4/$BiPO_4$	4	0.147	0.020	65.4	0.012	0.126	60.3
10.0% g-C_3N_4/$BiPO_4$	5	0.198	0.021	78.2	0.011	0.138	63.4
16.0% g-C_3N_4/$BiPO_4$	5	0.348	0.020	93.6	0.011	0.178	87.8
20.0% g-C_3N_4/$BiPO_4$	6	0.246	0.020	88.6	0.012	0.124	83.6

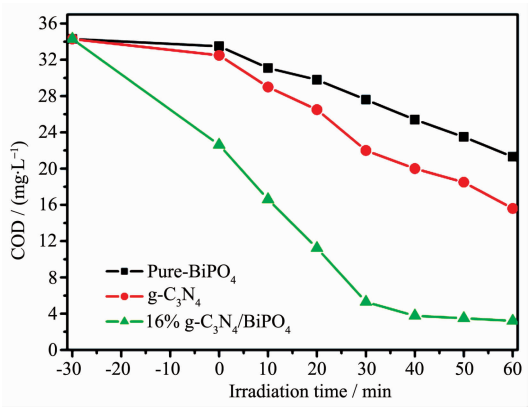

Fig.6 COD changes during the course of phenol photo-degradation in the presence of pure-$BiPO_4$, g-C_3N_4 and 16% g-C_3N_4/$BiPO_4$ heterojunctions

H_2O may occur slowly[19-20].

To demonstrate the potential applicability of g-C_3N_4/$BiPO_4$ photocatalyst, the stability of the 16% g-C_3N_4/$BiPO_4$ photocatalyst was investigated (Fig.7). After five cycles for photo-degradation of RhB, the catalyst did not exhibit obvious loss of activity, as shown in Fig.7a, confirming that g-C_3N_4 QDs decorated 1D rod-like $BiPO_4$ have high stability and are easy to be recycled. Fig.7b shows phases composition 16.0%g-C_3N_4/$BiPO_4$ did not after five cycles. Therefore, g-C_3N_4/$BiPO_4$ heterojunctions can be used as stable visible-light-responsive photocatalyst.

2.4 Possible photocatalytic mechanism of g-C_3N_4/$BiPO_4$ heterojunctions

To further investigate the reactive species in the degradation of RhB, TBA, BQ, and EDTA-2Na were introduced as the scavenger of ·OH, O_2^-· and h^+, respectively. Fig.8 shows the effects of different scavengers on the photocatalytic degradation of RhB

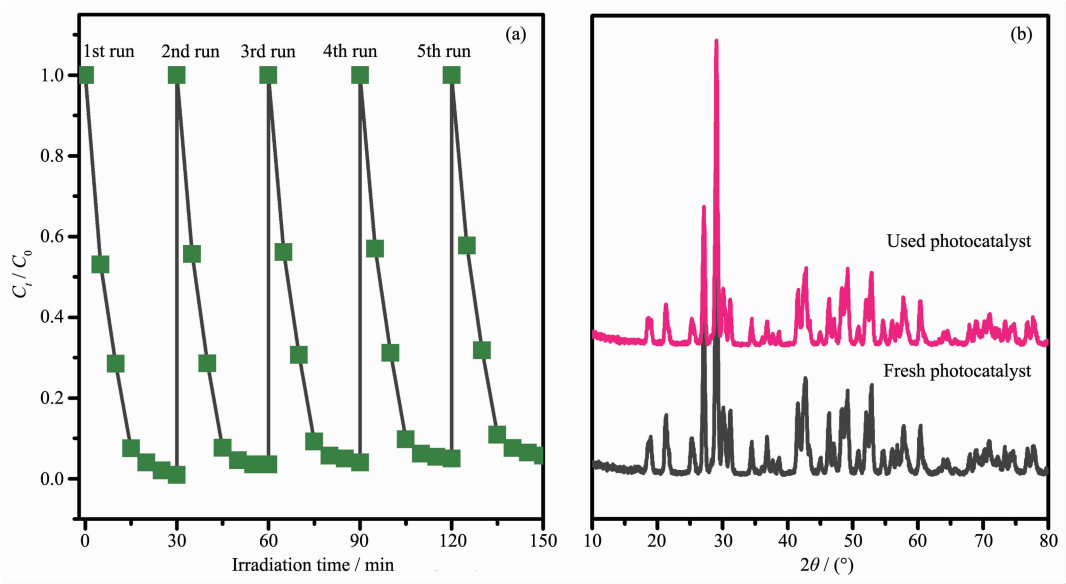

Fig.7 Repeated experiments of photocatalytic degradation of RhB on 16.0% g-C_3N_4/$BiPO_4$ photocatalyst under visible light irradiation (a) and XRD patterns of 16.0% g-C_3N_4/$BiPO_4$ photocatalyst before and after used for five cycles (b)

over 16% g-C_3N_4/$BiPO_4$. It can be seen that photocatalytic degradation of RhB was obviously suppressed by BQ and TBA, indicating that $O_2^{-}\cdot$ and ·OH are the main reactive species. As shown in Fig.8, there is also a slight change for RhB photocatalytic degradation when h^+ scavenger EDTA-2Na was added. This indicates that h^+ is also one of the reactive species involved in the RhB photocatalytic oxidation process.

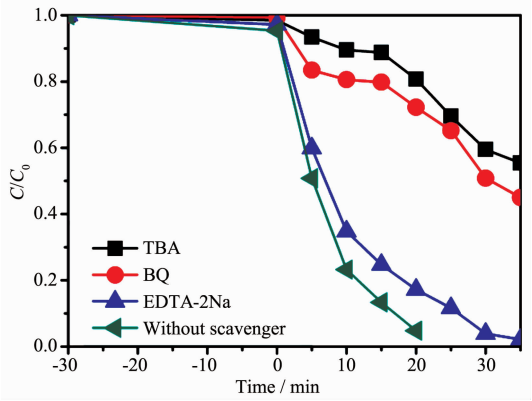

Fig.8　Photocatalytic degradation of RhB over 16% g-C_3N_4/$BiPO_4$ with the addition of scavengers

It is known that the generation of $O_2^{-}\cdot$ could be via two different processes. On the one hand, RhB can be excited by visible light to form the excited state (RhB*). RhB* then injects electrons into the CB of g-C_3N_4/$BiPO_4$ to form e_{CB}^-, which is scavenged by the O_2 on the surface of the catalyst to form $O_2^{-}\cdot$. So, it is reasonable that RhB may display a weak photosensitization effect on g-C_3N_4/$BiPO_4$ under visible light. On the other hand, when g-C_3N_4/$BiPO_4$ was irradiated under visible light, only g-C_3N_4 could be activated. The electrons and hole were photogenerated in CB and VB of g-C_3N_4, then move to the empty bottom of the CB of $BiPO_4$. Finally, the electron in the CB of $BiPO_4$ could react with O_2 to form $O_2^{-}\cdot$ (Fig.9). At the same time, ·OH may produced via followed reaction. Based on our experimental results and the discussions above, the mechanism of photocatalytic degradation of RhB on the g-C_3N_4/$BiPO_4$ heterojunctions may be proposed, as described in the Eq.(**1**)~(**12**):

$$RhB+h\nu \longrightarrow RhB^* \quad (1)$$

$$g\text{-}C_3N_4/BiPO_4+h\nu \longrightarrow g\text{-}C_3N_4/BiPO_4(e_{CB}^-+h_{VB}^+) \quad (2)$$

$$RhB^*+g\text{-}C_3N_4/BiPO_4 \longrightarrow g\text{-}C_3N_4/BiPO_4(e_{CB}^-) \quad (3)$$

$$g\text{-}C_3N_4/BiPO_4(e_{CB}^-)+O_2 \longrightarrow g\text{-}C_3N_4/BiPO_4+O_2^{-}\cdot \quad (4)$$

$$H_2O \longrightarrow H^++OH^- \quad (5)$$

$$O_2^{-}\cdot+2H^++e^- \longrightarrow H_2O_2 \quad (6)$$

$$H_2O_2+g\text{-}C_3N_4/BiPO_4\ (e_{CB}^-) \longrightarrow OH^-+\cdot OH \quad (7)$$

$$OH^-+h_{BV}^+[g\text{-}C_3N_4/BiPO_4] \longrightarrow \cdot OH+g\text{-}C_3N_4/BiPO_4 \quad (8)$$

$$H_2O+h^+ \longrightarrow \cdot OH+H^+ \quad (9)$$

$$RhB+h_{BV}^+\ [g\text{-}C_3N_4/BiPO_4] \longrightarrow \text{intermediate products} \quad (10)$$

$$RhB+O_2^{-}\cdot/\cdot OH \longrightarrow \text{intermediate products} \quad (11)$$

Simultaneous photocatalytic reaction:

$$\text{Intermediate products}+O_2^{-}\cdot/\cdot OH \text{ or } h_{BV}^+[g\text{-}C_3N_4/BiPO_4] \longrightarrow CO_2+H_2O+\cdots \quad (12)$$

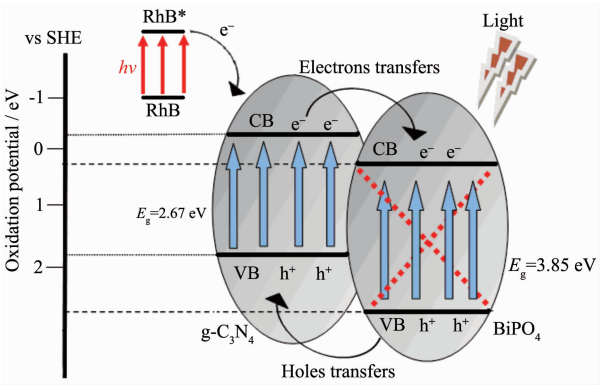

Fig.9　Potential of valence and conduction band for g-C_3N_4 and $BiPO_4$ to illustrate the photocatalytic enhancement mechanism of g-C_3N_4/$BiPO_4$ heterojunction

3　Conclusions

1D rod-like $BiPO_4$ micro crystals was synthesized via a hydrothermal. Then, g-C_3N_4 QDs with the size of about 20 nm were deposited on the surface of rod-like $BiPO_4$ by employing a followed impregnation-calcinations method to construct the novel g-C_3N_4/$BiPO_4$ heterojunctions. The g-C_3N_4 QDs decorated $BiPO_4$ exhibits enhanced photocatalytic activity in decomposition of RhB and phenol, which is much higher than that of pure-$BiPO_4$ and g-C_3N_4, and the content of g-C_3N_4 impacts the catalytic activity of g-C_3N_4/$BiPO_4$ heterojunction. The enhanced activity of as-fabricated g-C_3N_4/$BiPO_4$ heterojunctions is attributed to the efficient separation of electron-hole pairs in g-C_3N_4/$BiPO_4$ due to the formation of heterojunction between the surface of two semiconductors. Both $O_2^{-}\cdot$ and ·OH are main reactive species which responsible for the

decomposition of RhB and phenol. Furthermore, g-C_3N_4/$BiPO_4$ has high stability, suggesting that QDs decoration could be a promising strategy for designing new efficient photocatalyst.

References:

[1] Tong H, Ouyang S X, Bi Y P, et al. *Adv. Mater.*, **2012**,**24**(1): 229-251

[2] Kubacka A, Fernández-García M, Colón G. *Chem. Rev.*, **2012**,**112**(3):1555-1614

[3] Chen X B, Shen S, Guo L, et al. *Chem. Rev.*, **2010**,**110**(11): 6503-6570

[4] Liu J, Yang Q, Yang W T, et al. *J. Mater. Chem. A*, **2013**,**1** (26):7760-7766

[5] Wang W H, Himeda Y, Muckerman J T, et al. *Chem. Rev.*, **2015**,**115**(23):12936-12973

[6] Paola A D, García-López E, Marcì G, et al. *J. Hazard. Mater.*, **2012**,**211-212**:3-29

[7] Kudo A, Miseki Y. *Chem. Soc. Rev.*, **2009**,**38**(1):253-278

[8] Cheng H. F, Huang B B, Wang P, et al. *Chem. Commun.*, **2011**,**47**(25):7054-7056

[9] Wang Y J, Guan X F, Li L P, et al. *CrystEngComm*, **2012**,**14** (23):7907-7914

[10]Wang D J, Zhang J, Guo L. *J. Inorg. Mater.*, **2015**,**30**(7):683 -693

[11]Lin X P, Xing J C, Wang W D, et al. *J. Phys. Chem. C*, **2007**,**111**(49):18288-18293

[12]Geng J, Hou W H, Lü Y N, et al. *Inorg. Chem.*, **2005**,**44** (23):8503-8509

[13]Xu H, Xu Y G, H. Li M, et al. *Dalton Trans.*, **2012**,**41**(12): 3387-3394

[14]Wang X C, Meada K, Thomas A, et al. *Nat. Mater.*, **2009**,**8** (1):76-80

[15]Wang Y, X. Wang C, Antonietti M. *Angew. Chem. Int. Ed.*, **2012**,**51**(1):68-89

[16]Pan C S, Xu J, Wang Y J, et al. *Adv. Funct. Mater.*, **2012**, **22**(7):1518-1524

[17]Li Z S, Li B L, Peng S H, et al. *RSC Adv.*, **2014**,**4**(66): 35144-35148

[18]Wang D J, Guo L, Zhen Y Z, et al. *J. Mater. Chem. A*, **2014**,**2**(10):11716-11727

[19]WANG Dan-Jun(王丹军), YUE Lin-Lin(岳林林), ZHANG Jie(张洁), et al. *J. Synth. Cryst.*(人工晶体学报), **2014**,**43** (1):2977-2984

[20]Zhang L S, Wong K H, Chen Z G, et al. *Appl. Catal. A*: *Gen.*, **2009**,**363**(1/2):221-229

[21]Wang Y J, Lin J, Zong R L, et al. *J. Mol. Catal. A*: *Chem.*, **2011**,**349**(1/2):13-19

[22]Lin H L, Cao J, Luo B D, et al. *Chin. Sci. Bull.*, **2012**,**57** (22):2901-2907

[23]Li F T, Zhao Y, Hao Y J, et al. *J. Hazard. Mater.*, **2012**,**239** -**240**:118-127